

T-3DGS: Removing Transient Objects for 3D Scene Reconstruction

Vadim Pryadilshchikov¹ Alexander Markin¹ Artem Komarichev¹ Ruslan Rakhimov²
Peter Wonka³ Evgeny Burnaev^{1,4}

¹Skoltech, Russia ²Robotics Center, Russia ³KAUST, Saudi Arabia ⁴AIRI, Russia

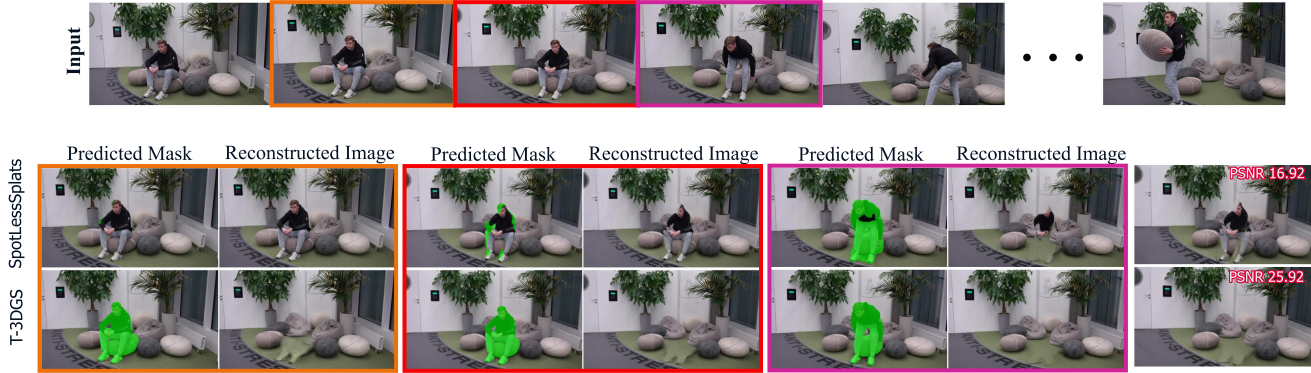


Figure 1. Recent state-of-the-art methods, e.g. SpotLessSplats [34], often fail to correctly identify masks for transient / semi-transient objects. Our proposed *T-3DGS* method successfully locates all transient distractors, extracts clean masks, and propagates them between frames. By masking transient objects, *T-3DGS* can produce clean reconstruction results with high-fidelity novel view synthesis on a given sequence of images or videos captured in the wild.

Abstract

We propose a novel framework to remove transient objects from input videos for 3D scene reconstruction using Gaussian Splatting. Our framework consists of the following steps. In the first step, we propose an unsupervised training strategy for a classification network to distinguish between transient objects and static scene parts based on their different training behavior inside the 3D Gaussian Splatting reconstruction. In the second step, we improve the boundary quality and stability of the detected transients by combining our results from the first step with an off-the-shelf segmentation method. We also propose a simple and effective strategy to track objects in the input video forward and backward in time. Our results show an improvement over the current state of the art in existing sparsely captured datasets and significant improvements in a newly proposed densely captured (video) dataset. More results and code are available at <https://transient-3dgs.github.io>.

1. Introduction

Novel view synthesis and 3D scene reconstruction from multiple 2D images or videos have emerged as rapidly evolving research areas within computer vision. Neural Ra-

diance Fields (NeRF) [21] and, more recently, 3D Gaussian Splatting (3DGS) [12] have shown remarkable improvements in novel view synthesis on complex scenes. NeRF implicitly represents the scene as a volumetric function, and 3DGS explicitly represents it as a set of 3D Gaussians. Both approaches produce high-quality realistic images. There are multiple follow-up works for diverse downstream applications including 3D scene reconstruction [9, 16, 44], 3D synthesis [25, 39, 48], semantic and language integration into 3D representations [13, 36, 37], etc.

Both 3D Gaussian Splatting and NeRF optimize 3D scene reconstruction using photometric losses. High-quality results are achieved under the assumption that the captured scene is completely static and does not include any *distractors*, such as moving objects (i.e. transient objects), shadows, lightning changes, etc. However, in real-world scenarios, such an assumption can hardly be satisfied. The recordings, even when captured carefully, often contain moving people, cars, or other dynamic objects with their shadows, especially in locations that are tourist landmarks. Ignoring distractors during scene optimization leads to undesired blurring effects and floating artifacts. At the same time, removing such distractors from the cap-

tured recordings is challenging and limits NeRF and 3DGS widespread usage. The process of manual annotations of distractors is labor-intensive. Another approach is to utilize pre-trained segmentation models to locate transient distractors. This approach has two main limitations: 1) it needs prior knowledge of transients as a semantic class, and 2), more importantly, existing segmentation models cannot distinguish between static and dynamic objects of the same semantic class. Additionally, we would like to identify semi-transient objects in recordings and remove them from the scene. We define a semi-transient object as an object that has both dynamic and static states during the capturing process, e.g. a pushed chair stops after some time and becomes a fully static object. Therefore, we need more robust identification methods for transient and semi-transient distractors throughout the captured recordings.

In our work, we introduce a novel T-3DGS approach to 3D static scene reconstruction with 3DGS from a monocular video taken in uncontrolled setting. Our method comprises two main components: an unsupervised transient detector and a transient mask propagation framework. Firstly, as it was observed previously [31, 34], relying only on image residuals in transient identification is not a robust approach, e.g., due to appearance changes and color similarity between transient objects and background. We need more robust features, which are semantically consistent as well as novel architecture and loss design. Our proposed transient network is trained concurrently on both rendered (reconstructed) images and reference images through novel robust regularization losses. It utilizes semantically consistent features and is capable of producing more accurate masks with fewer misidentifications of transient objects, and significantly reduces the number of falsely identified objects as dynamic objects. Secondly, we have shown in our experiments that concurrent works [34, 43] fail to identify the semi-transient distractors and remove them from the scene as shown in Fig. 1. We further introduce our mask propagation framework that allows the extraction of object-aware masks that are consistent throughout the video and are especially helpful in improving the consistency of semi-transient distractor masks. Overall, our method remains robust for any type of distractors present in the scene. Lastly, we have collected a novel *T-3DGS dataset* containing several challenging scenes filled with semi-transient and slow-moving objects with dense frame rates. We evaluate our approach on casually captured scenes [31, 33] and on our semi-transient dataset. Our method consistently outperforms state-of-the-art approaches in reconstruction quality.

Our key contributions include:

- A novel transient network to identify dynamic distractors utilizing features from a visual foundation model.
- A novel video object segmentation module that robustly tracks objects throughout the video regardless of the

frame rate and semi-transient behavior.

- A novel challenging dataset that contains diverse scenes with semi-transient distractors and scenes with slow-moving objects for evaluation.
- Our proposed method presents new state-of-the-art performance on robust reconstruction of the static scene parts on standard benchmark datasets.

2. Related Work

We briefly review Neural Radiance Fields and 3D Gaussian Splatting works with a focus on removing non-static distractors in the scene.

Neural Radiance Fields (NeRFs) [21] have emerged as a widely adopted method for high-quality scene reconstruction and novel view synthesis of 3D scenes. There are several follow-up extensions of NeRFs for fast training and inference [3, 22, 38], novel view synthesis on dynamic scenes [24, 26, 42], training on single or limited views [11, 30]. The seminal paper 3D Gaussian Splatting [12] employs Gaussian primitives to model scenes instead of relying on continuous volumetric representations. This method has recently gained popularity as a faster alternative to NeRFs. Follow-up works have extended 3DGS in many directions, for instance in dynamic [47, 52] and static [20, 50] scenes, utilizing additional information such as depth [55].

Handling Distractors in NeRFs. NeRF-W [19] and RobustNeRF [33] are two pioneering works similarly approaching the problem of handling transient distractors by utilizing photometric error. NeRF-W reconstructs both static background and transients combined with a data-dependent uncertainty field. RobustNeRF utilizes Iteratively Reweighted Least Squares for transient object identification and removal. Both methods rely directly on color residual supervision and often misclassify transient objects and backgrounds with similar colors. Additionally, they both require careful hyper-parameters tuning. Another alternative approach is NeRFBusters [46], which uses a data-driven prior to remove artifacts. NeRF On-the-go [31] utilizes DINOv2 features [23] to identify and eliminate distractors by predicting uncertainties through a shallow MLP and can deal with more complex scenes than RobustNeRF. NeRF-HuGS [2] utilizes two types of heuristics: 1) COLMAP-based [35] features combined with SAM [14] and 2) residual-based heuristics to identify and remove transient distractors. Their method is not robust to heavy transient distractions because both heuristics are not stable under such conditions, as shown in [31].

Extracting Features from Vision Foundation Models.

Vision Foundation Models (VFs) are trained on large-scale data to perform strong generalization ability to unseen domains or novel tasks. For example, there are a set of task-specific foundation models for image classifica-

tion [7, 17, 41], for segmentation [14, 29], and depth prediction [51] tasks. Task-agnostic models trained through self-distillation like DINO [1, 23] learn features that can be generalized for multiple vision tasks. CLIP [27] is a weakly-supervised multi-modal model that learns visual concepts from natural language supervision by contrastive pre-training on image-text pairs and performs zero-shot transfer to a wide range of downstream tasks. The features from Diffusion Models [10, 32] have also been used for semantic or keypoint correspondence [18, 40, 54]. In our work, we aim to utilize features from foundation models to identify transient distractors more robustly. We propose to use DINOv2 features [23] because they are semantically meaningful and spatially consistent, which is crucial for reliable distractor identification.

Video Object Segmentation. The goal of semi-supervised VOS is to identify when an object appears for the first time and then track it throughout the video. There are several recent approaches based on transformers [4, 5]. However, current methods suffer from mask inconsistencies throughout the video, especially when objects disappear from the video and reappear later. Additionally, current methods assume that the input is provided with a high frame rate, and these methods are not stable when the frame rate is low. In our work, we address these shortcomings.

Handling Distractors in 3DGS. There are multiple works addressing training 3DGS on unconstrained in-the-wild photo collections. SWAG [6] improves robustness of 3DGS by learning an appearance embedding space and image-dependent opacity variations to handle transient objects better. Gaussians in the Wild (GS-W) [53] utilizes CNN features to capture dynamic and intrinsic appearances from a reference image. Wild-GS [49] explicitly learns appearance embeddings by sampling the triplane from the reference image. Robust 3DGS [43] proposes a self-supervised approach to identify transient distractors by utilizing image residuals and leveraging a pre-trained segmentation network to produce object-aware masks. SpotLessSplats [34] proposes a method to identify transient objects by utilizing pre-computed feature maps from a foundation model [40] coupled with a robust optimization of 3DGS. These works [6, 34, 43, 49, 53] suffer from 1) hyper-parameter tuning, i.e., threshold parameters, 2) predicting inaccurate transient masks across the video and 3) relying on image residuals that result in falsely detecting transients as shown in Fig. 1. In our approach we try to address the limitations of the current works by identifying transients more accurately and consistently between video frames.

3. Method

We propose a novel approach for reconstructing static scenes from unconstrained videos containing dynamic objects using 3D Gaussian Splatting (3DGS). Our method, il-

lustrated in Fig. 2, introduces two key components to handle dynamic objects effectively: (1) **transient mask predictor (TMP)** and (2) **transient mask refiner (TMR)**. The transient area detection component, implemented through our transient mask learning predictor, identifies regions containing dynamic objects by predicting per-pixel probabilities using semantic features, enhanced with a novel consistency regularization term. This regularization reduces false positive predictions while maintaining accurate detection of dynamic objects. The transient mask propagator component improves transient detection in both the spatial and temporal domain by leveraging SAM2 [29] to propagate transient masks across different frames, enabling artifact-free reconstruction.

3.1. 3D Gaussian Splatting

We base our method on 3DGS [12]. Given a set of posed images $\{I_n\}_{n=1}^N, I_n \in \mathbb{R}^{H \times W \times C}$, 3DGS represents a 3D scene as a set of anisotropic Gaussians $\{\mathcal{G}_i\}$, where each Gaussian is represented by its position (mean) μ_i , a positive semi-definite covariance matrix Σ_i , an opacity α_i , and a view-dependent appearance component (color) parametrized by spherical harmonics (SH) [28]. 3DGS representation is learned through optimization of Gaussian parameters via stochastic gradient descent.

Each 3D Gaussian is projected onto the image plane through a differentiable rasterization process to render an image from a specific viewpoint. First, the 3D Gaussian's covariance matrix Σ_i is projected to obtain a 2D covariance matrix Σ'_i in screen space: $\Sigma'_i = JW\Sigma_iW^TJ^T$, where W is the perspective transformation matrix and J is the Jacobian of the projection matrix. The projected 2D Gaussian's contribution to each pixel (x, y) is then computed as: $\alpha_i = \exp(-\frac{1}{2}(p - \mu'_i)^T(\Sigma'_i)^{-1}(p - \mu'_i))$, where p is the pixel coordinate and μ'_i is the projected mean. The final color at each pixel is obtained through alpha compositing of all contributing Gaussians, sorted by depth: $C = \sum_{i=1}^M T_i \alpha_i c_i$, where $T_i = \prod_{j < i} (1 - \alpha_j)$ is the accumulated transmittance, c_i is the view-dependent color computed from spherical harmonics coefficients, and M is the number of Gaussians contributing to the pixel.

3.2. Transient Mask Prediction

Given the input images $\{I_n\}_{n=1}^N$, the goal is to optimize unsupervised *TMP* through 3DGS reconstruction to identify transient distractors without explicit supervision as shown in Fig. 2. The training process consists of two steps: (1) optimizing the 3DGS parameters while keeping the *TMP* frozen, and (2) optimizing the *TMP* while keeping the 3DGS parameters frozen. After each iteration, both models' weights are updated. The *TMP* is trained to identify transient objects without explicit supervision, purely from the reconstruction objectives. Several recent

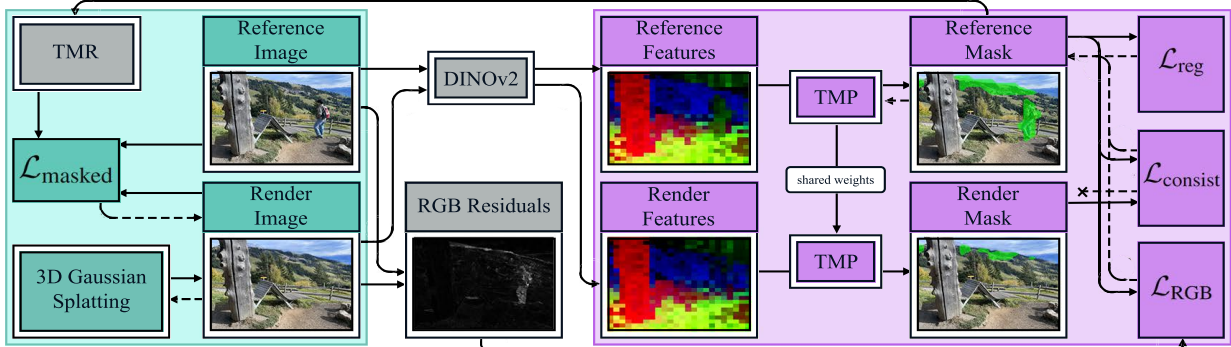


Figure 2. The architecture of the proposed method. We use a modified version of 3D Gaussian Splatting (in green), with masked loss term $\mathcal{L}_{\text{masked}}$ specified in (Eq. 6). Every iteration, we begin by rendering a reconstruction of a randomly sampled reference image. Then we calculate RGB color residuals (i.e. L_1 difference of those images), and DINOv2 features of both images. These features are then fed to our *TMP* model (in purple) that predicts binary masks for both reference and rendered images (shown in green on the actual images for clarity). We then calculate the loss specified in (Eq. 1) and update the parameters of the *TMP* via backpropagation, denoted with dashed lines. Notably, we detach rendered image masks to prevent the *TMP* from learning on features of the rendered image. Additionally, we use a SAM-based mask propagation module, as it further increases the consistency and sharpness of masks.

works [6, 8, 15, 34, 49] follow a similar approach, which has demonstrated the effectiveness of such optimization for handling dynamic scenes.

Following [15, 34], we reformulate the transient detection problem as a semantic feature classification task rather than a direct pixel-level prediction. This approach leverages pre-trained foundation models to extract rich semantic features from images, enabling our system to make decisions based on high-level semantic understanding rather than solely relying on color information. This semantics-aware approach proves to be more robust in distinguishing between static and transient objects compared to traditional color-based methods. One of our main contributions is the unsupervised consistency loss in Eq. 3.

3.2.1 Feature Extraction

For each training iteration, we extract DINO v2 features [23] from both the input image I and corresponding rendering \hat{I} producing feature maps f, \hat{f} respectively. We choose DINO v2 for several key reasons: (1) its self-supervised training enables robust semantic understanding without class-specific biases, (2) it demonstrates strong performance in distinguishing object boundaries and semantic regions even for previously unseen objects, (3) compared to alternatives like DIFT [40] features, DINO v2 offers significantly faster computation times, making it more practical for iterative training processes. These features provide a rich foundation for our *TMP* to make accurate decisions about scene dynamics without explicit supervision.

3.2.2 Transient Probability Masks

The extracted features are processed through our *TMP* module, which implements logistic regression to compute per-

feature probability masks: $P^f = \sigma(\mathbf{W}f)$, where $\sigma(\cdot)$ is the sigmoid function, \mathbf{W} represents the *TMP* weights. Since the features are patch-wise (14×14 px), we upsample predicted probability masks P^f and \hat{P}^f to the original image resolution using bilinear interpolation, obtaining pixel-wise transient masks P and \hat{P} respectively. Notably, *TMP* learns to distinguish transient objects without explicit supervision, guided only by the optimization objectives described below.

3.2.3 Loss Function

The *TMP* is optimized using three complementary losses:

$$\mathcal{L}_{\text{transient}} = \mathcal{L}_{\text{RGB}} + \lambda_{\text{prior}} \mathcal{L}_{\text{reg}} + \mathcal{L}_{\text{consist}}, \quad (1)$$

The RGB loss identifies regions where the rendered image differs from the ground truth: $\mathcal{L}_{\text{RGB}} = \left\| (1 - P) \odot (I - \hat{I}) \right\|_1$, where $\|\cdot\|_1$ denotes the L_1 norm, and \odot represents the element-wise (Hadamard) product. This loss exploits the observation that dynamic objects typically create larger discrepancies between rendered and ground truth images. By weighting these differences with $(1 - P)$, we encourage the classifier to assign higher transient probabilities to regions showing significant reconstruction errors.

The regularization term promotes sparse predictions: $\mathcal{L}_{\text{reg}} = \|P\|_1$. This sparsity constraint helps produce compact, focused masks while reducing false positives.

Previous works [8, 49] used a sum of \mathcal{L}_{RGB} and $\lambda_{\text{prior}} \mathcal{L}_{\text{reg}}$ without the consistency loss, which has an explicit solution. For each pixel (i, j) , the optimal solution has the form:

$$P_{i,j}^* = \begin{cases} 1 & \text{if } |I_{i,j} - \hat{I}_{i,j}| > \lambda_{\text{prior}} \\ 0 & \text{if } |I_{i,j} - \hat{I}_{i,j}| \leq \lambda_{\text{prior}} \end{cases} \quad (2)$$

However, this methodology exhibits significant limitations when reconstructing geometrically complex static structures. In such cases, even static objects may generate RGB errors exceeding λ_{prior} due to reconstruction challenges, leading to their erroneous classification as dynamic elements and subsequent masking. This misclassification ultimately results in degraded reconstruction quality of the static scene components. To address these limitations, additional regularization constraints are necessary.

Our novel consistency term prevents misclassification in challenging regions:

$$\mathcal{L}_{\text{consist}} = \left\| P \odot \hat{P} \right\|_1. \quad (3)$$

This term addresses cases where static objects with complex surfaces might show high reconstruction error while being semantically consistent. The underlying principle is that while geometric complexity may lead to reconstruction errors in RGB space, the semantic features of static objects remain consistent between input and rendered images. By penalizing overlap between input and rendered image masks (P and \hat{P}), we encourage the detector to focus on genuine semantic differences rather than reconstruction artifacts.

Fig. 3 demonstrates the effectiveness of this approach: after 7000 iterations, the model with consistency loss produces precise masks for transient objects in the input image while generating minimal masks for the rendered image. In contrast, without the consistency term, the *TMP* exhibits numerous false positives in both input and rendered images, often misclassifying poorly reconstructed static regions as transient objects. This behavior validates that the consistency loss effectively distinguishes between genuine dynamic objects and reconstruction artifacts based on their semantic representations.

3.2.4 Training Stability

To ensure stable training, we implement several key strategies. First, we detach \hat{P} from the computational graph during consistency loss computation to prevent the model from learning to distinguish between ground truth and rendered images.

During 3DGS optimization, there are periods when renders may be unreliable: at the beginning of training and after each opacity reset. Following [15], we address this by implementing two key strategies. First, we delay the start of *TMP* training until the 3DGS optimization has completed its first 500 iterations, ensuring the initial scene reconstruction has reached sufficient quality. Second, after each opacity reset, we temporarily pause the *TMP* optimization for 250 iterations while keep training 3DGS, allowing the reconstruction to stabilize before resuming transient detection.

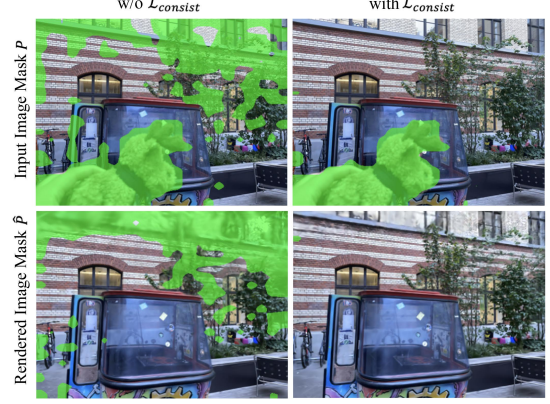


Figure 3. The comparison of the *TMP* predictions with and without $\mathcal{L}_{\text{consist}}$ term. The quality of the predicted transient masks for the input image with consistency loss term is significantly better than without this term. The predicted masks by *TMP* are shown in green color.

Prior to bilinear interpolation, we dilate the masks by one pixel. This dilation step serves two purposes: it compensates for the coarse feature resolution of the foundation model (which processes images in patches) and helps address imprecise boundary predictions.

These modifications ensure robust training and accurate transient object detection across diverse dynamic scenes.

3.3 Transient Mask Refinement

Our transient area detection pipeline is robust for current benchmarks, where transient object is always dynamic and changes its position from frame to frame. But for semi-transient objects, which may do not change position for some frames it fails and masks only parts of video when it's dynamic. To address these issue, we introduce a masks propagation process that refines transient masks into temporally consistent, accurate masks with high-resolution boundaries across the entire video sequence through refinement and propagation. Each segmentation consists of a binary mask defining the object's spatial extent and a unique label that remains consistent throughout the video sequence.

3.3.1 Spatial Refinement

We employ the Segment Anything Model (SAM) [14] to refine our transient maps P_i into more precise masks M'_i . For each connected component C_i^k in P_i , we sample up to ten points as prompts for SAM, leveraging its ability to generate high-quality segmentations from sparse inputs to extract a set of object-aware masks $M'_i = \{M'^j_i\}_{j=1}^{L_i}$, where L_i is the number of predicted masks for image I_i . Due to potential inaccuracies in the boundaries of our masks, some sampled points might occasionally fall on the background

rather than the object itself (e.g., a point sampled between the legs of a person). To address this issue, we filter the predicted masks based on their local coverage score:

$$CS_{\text{local},i} = \frac{|P_i \cap M'_i|}{|M'_i|} \quad (4)$$

We keep only masks that satisfy $CS_{\text{local},i} > \lambda_{\text{cov}}^{\text{ref}}$, forming the refined set $M'_i = \{M'_i | CS_{\text{local},i} > \lambda_{\text{cov}}^{\text{ref}}\}$.

3.3.2 Temporal Refinement

To address potential false negatives, we propagate the refined masks $\{M'_i\}_{i=1}^N$ throughout the video using SAM2 [29] to obtain more consistent masks $\{M_i\}_{i=1}^N$. Our propagation process consists of three stages:

1. Forward Propagation: Iterating from the first to the last frame, to propagate segmentation masks forward.
2. Backward Propagation: Iterating Last-to-first frame, to propagate information from future frames backwards.
3. Final Propagation: Final Propagation: A final first-to-last pass, considering both past and future frames as context, which helps resolve any temporal inconsistencies.

To manage computational resources efficiently, we introduce a memory size parameter N_m , which limits the number of frames considered during propagation. At each step, we only maintain and use the segmentations from the N_m most nearest frames, balancing between temporal consistency and memory constraints.

Throughout propagation, we manage mask intersections to ensure coherent segmentation. For any pair of masks M_i^l and M_i^m with $IoU(M_i^l, M_i^m) > \lambda_{\text{merge}}$, we merge them into a single mask, assigning the lower of the two original labels to maintain consistency.

3.3.3 Dynamic Object Filtration

To filter out false positive transients and ensure robust detection, we introduce a Stability Ratio (SR) metric that combines both spatial overlap accuracy and temporal consistency. For each detected object, the SR is calculated as $SR = \frac{1}{N} \sum_{i=1}^N (R_i \cdot CS_{\text{global},i})$, where N is the number of valid frames, R_i is the mean value of the absolute difference between ground truth and rendered images within the masked region in frame i , and $CS_{\text{global},i} = |P_i \cap M_i| / |M_{\max}|$ is the global coverage score. Here, P_i represents the prompt mask in frame i , M_i is the segmentation mask, and M_{\max} is the maximum size of the object mask across all frames. This global score helps evaluate the object's consistency relative to its largest observed size. A frame is considered valid and contributes to the SR calculation only if its local coverage score (Eq. 4) exceeds the validation threshold $\lambda_{\text{cov}}^{\text{val}}$. Objects with SR below a threshold λ_{SR} are filtered out as potential false detections. This

dual coverage score system ensures that objects maintain both spatial accuracy through local coverage and temporal consistency through global coverage and difference image values.

3.4 Artifact-Free Reconstruction

3DGS tends to generate floating artifacts ("floaters") near the camera, particularly in challenging regions like those identified by transient masks. These artifacts can saturate gradients and degrade overall reconstruction quality. We address this issue through depth-aware regularization.

We render depth D for each pixel using alpha compositing similar to color rendering: $D = \sum_{i=1}^M T_i \alpha_i d_i$, where d_i is the depth value of the i -th Gaussian, T_i is the accumulated transmittance, and α_i is the opacity value. To suppress floating artifacts while preserving sharp depth discontinuities at object boundaries, we apply anisotropic total variation (TV) regularization to the rendered depth maps: $\mathcal{L}_{\text{depth}} = \text{mean}(|\nabla_x D|) + \text{mean}(|\nabla_y D|)$, where p indexes over pixels, ∇_x and ∇_y are spatial gradients in x and y directions respectively.

3.5 Masked Gaussian Splatting Optimization

The final step involves training the Gaussian Splatting model with the obtained masks $\{M_i\}_{i=1}^N$ for transients. Let M_i be the binary mask for frame i , defined as:

$$M_i(x, y) = \begin{cases} 1 & \text{if } (x, y) \text{ is in an occluded area} \\ 0 & \text{if } (x, y) \text{ is in a static area,} \end{cases} \quad (5)$$

where (x, y) represents pixel coordinates in the image. We apply binary dilation to M_i for N_e iterations, yielding M_i^* . This operation creates a buffer zone around detected dynamic objects, enhancing the robustness of our static scene reconstruction. The final loss for 3DGS is:

$$\mathcal{L}_{\text{masked}} = \lambda_{\text{SSIM}} \cdot L_{\text{SSIM}}(I_i \odot \overline{M}_i^*, \hat{I}_i \odot \overline{M}_i^*) + \lambda_{\text{LI}} \cdot \left\| \overline{M}_i^* \odot (I_i - \hat{I}_i) \right\|_1 + \lambda_{\text{depth}} \mathcal{L}_{\text{depth}}, \quad (6)$$

where I_i , \hat{I}_i , $\mathcal{L}_{\text{depth}}$, \odot and $\|\cdot\|_1$ are the same as were defined previously, L_{SSIM} is a structural similarity loss, \overline{M}_i^* is a negation of M_i^* that represents static background and λ_{SSIM} , λ_{LI} and λ_{depth} are weighting factors.

This formulation allows the model to focus on static scene elements, effectively handling dynamic objects in the reconstruction process. By integrating these steps, our method robustly reconstructs static scenes from unconstrained videos, effectively handling transient distractors.

4 Experiments

We evaluate our proposed T-3DGS model on various datasets captured in uncontrolled settings and filled with diverse distractors. We perform qualitative and quantitative

	Mountain		Fountain		Corner		Patio		Spot		Patio High		Mean	
	PSNR ↑	SSIM ↑												
NeRF On-the-go [31]	20.15	0.64	20.11	0.61	24.22	0.81	20.78	0.75	23.33	0.79	21.41	0.72	21.67	0.72
3DGS [12]	20.09	0.70	20.11	0.69	23.51	0.85	15.87	0.68	20.78	0.80	17.80	0.69	19.69	0.74
Robust3DGS [43]	16.97	0.61	18.18	0.59	23.47	0.85	21.33	0.85	22.61	0.88	21.81	0.82	20.73	0.77
WildGaussians [15]	20.77	0.70	20.74	0.67	25.79	0.88	21.77	0.85	24.39	0.88	22.36	0.80	22.64	0.80
SpotLessSplats [34]	21.25	0.66	20.49	0.63	25.59	0.85	21.13	0.80	24.13	0.78	22.18	0.76	22.46	0.75
Ours	20.89	0.72	21.01	0.69	26.64	0.90	21.55	0.86	25.96	0.91	23.18	0.84	23.21	0.82

Table 1. Quantitative comparison on *On-the-go* dataset [31].

	Lab 1		Lab 2		Library		Anti-Stress		Office		Mean	
	PSNR ↑	SSIM ↑										
3DGS [12]	24.49	0.91	20.42	0.87	20.08	0.89	20.45	0.86	26.96	0.94	22.48	0.89
Robust3DGS [43]	25.35	0.93	24.74	0.92	24.33	0.93	22.95	0.91	28.52	0.96	25.18	0.93
WildGaussians [15]	25.71	0.92	23.68	0.91	24.65	0.92	21.69	0.89	28.89	0.95	24.92	0.92
SpotLessSplats [34]	25.28	0.91	24.63	0.90	24.11	0.91	22.22	0.90	28.08	0.92	24.86	0.91
Ours w/o TMR	25.69	0.93	24.74	0.92	23.82	0.92	24.21	0.92	29.01	0.95	25.49	0.93
Ours w/ TMR	27.71	0.95	25.42	0.93	28.34	0.97	28.79	0.97	29.87	0.96	28.03	0.96

Table 2. Quantitative comparison on our *T-3DGS* dataset.

comparisons of our method with other SOTA methods. Finally, we provide an ablation study of our design and loss choices and discuss the limitations of the proposed method.

Datasets. We evaluate our model on three challenging datasets. The *NeRF On-the-go dataset* [31] contains 4 outdoor and 2 indoor sparsely captured scenes with different levels of occlusions (from 5% to over 30%) and minimal changes in appearance. The *RobustNeRF dataset* [33] contains 5 indoor scenes with unintentional changes during the capture process. Those changes include both transient objects that appear and disappear without forming a coherent video sequence (i.e., do not have a clear temporal ordering) and dynamic objects (e.g., floating balloons). Additionally, we introduce our novel *T-3DGS dataset*. The dataset contains 5 densely captured indoor scenes. Generally, dynamic objects in our videos are walking people and various small objects. However, unlike previous datasets, all scenes include various adversarial cases, such as transient, semi-transient, and slow-moving objects.

Baselines. We compare our model against vanilla 3D Gaussian Splatting [12] and against the current state-of-the-art method SpotLessSplats [34]. We further include WildGaussians [15] and Robust3DGS [43] as baselines. To compare different models we adopt commonly used PSNR and SSIM [45] metrics for evaluation.

Implementation details. All our experiments are conducted following the training setup from the official 3DGS implementation. We train our models for 30K iterations, using the Adam optimizer with a learning rate of 1e-3 for the *TMP*. The depth regularization loss $\mathcal{L}_{\text{depth}}$ is activated after the first 500 iterations, allowing the 3DGS to establish initial geometry reconstruction. For the experiments with mask propagation, we first train the *TMP* for 7000 iterations. At that point we pause the training to propagate the transient masks. Subsequently, we initiate a new training procedure using the propagated masks, keeping all other parameters the same as the original training setup. Thanks to

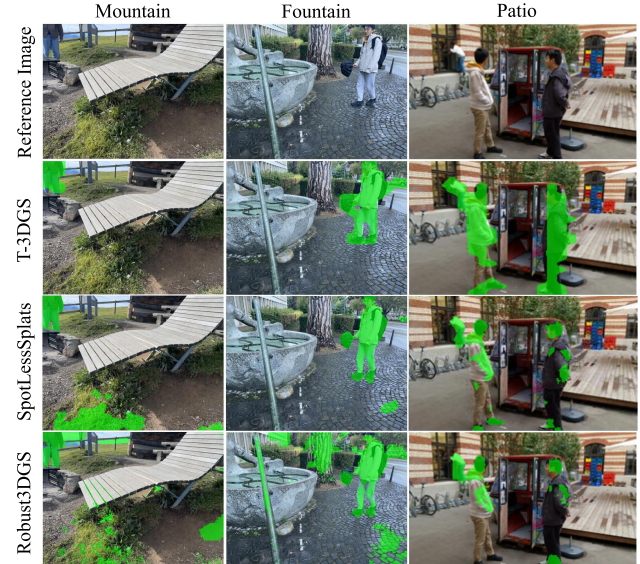


Figure 4. Qualitative results on the *On-the-go* dataset. Our method detects transient objects better than our competitors. Predicted masks are shown in green.

our consistency term, we achieve robust results with a fixed regularization parameter $\lambda_{\text{prior}} = 0.1$ across all scenes, eliminating the need for per-scene parameter tuning that was required in previous approaches.

4.1. Quantitative Comparisons

We evaluate our model on all three datasets. We report results on *On-the-go* and *T-3DGS* datasets in Tab. 1 and 2, respectively, and we move evaluation results on *RobustNeRF* dataset to Supplementary Material as it is the least challenging. As shown in Tab. 1 and 2 our method generally outperforms current SOTA methods, in particular, our method is robust to changes in distant and high-frequency details. In Tab. 1 we run our method directly on masks predicted by

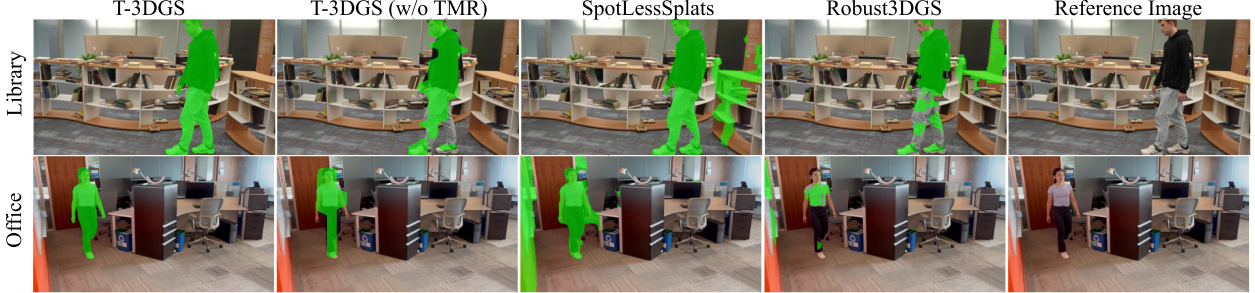


Figure 5. Qualitative results on *T-3DGS* dataset. Our method detects cleaner transient masks and improves them further by mask propagation *TMR* module. Predicted masks are shown in green.

TMP module without mask propagator.

While current SOTA methods struggle to detect semi-transient objects (Tab. 2), our proposed transient network *TMP* achieves higher performance minimizing false predictions. The integration of the SAM-based mask propagation *TMR* module further enhances our results in scene reconstruction filled with semi-transient objects, providing more accurate and reliable reconstructions.

4.2. Qualitative Comparisons

For qualitative comparison, we compare our method to SpotLessSplats [34] and Robust3DGS [43]. Fig. 4 and 5 show that our method has very few false negatives and robustly detects transients. For example, on the On-the-go dataset most of the methods struggle with high-frequency details and distant objects, as both generally reconstruct slower than the rest of the scene, and therefore confuse RGB residuals-based and similar methods. However, due to the introduction of our robust loss, such artifacts generally disappear from our dynamic maps. While our masks are less sharp, as we upsample them from low-resolution DINOv2 patches, techniques such as guided upsampling can improve performance of our method, however we leave this topic to following works. It should be noted, that SpotLessSplats [34] use features obtained from higher-resolution images, while we compute our features on a lower resolution, the same resolution used for training 3DGS.

For our *T-3DGS* dataset, we additionally utilize the SAM-based mask propagation module to propagate object-aware masks for semi-transient objects as shown in Fig. 5. While most methods would benefit from such a technique in principle, our masks have higher quality and fewer wrong detections. Applying mask propagation to other methods risks propagating errors.

4.3. Ablation Study

We show the importance of each component in our *T-3DGS* model, separately disabling each of them. We report ablation results in Tab. 3 on *On-the-go* dataset. In the first

	<i>On-the-go</i> dataset	
	PSNR \uparrow	SSIM \uparrow
w/o dilation	22.65	0.82
w/o $\mathcal{L}_{\text{consist}}$	16.76	0.69
w/o $\mathcal{L}_{\text{depth}}$	23.02	0.82
Ours (full)	23.21	0.82

Table 3. We ablate the importance of each component of our method on *On-the-go* dataset. We report the mean over all scenes.

experiment, we show the importance of the dilation before upsampling per-feature probability masks P^f . Without dilation the produced masks keep shrinking during the optimization process. This leads to a quality reduction in the renderings. In the second experiment, we turn off consistency loss term $\mathcal{L}_{\text{consist}}$. Our results show that adding this loss term improves the quality of renderings across all datasets. In our last experiment, we ablate the regularization term on depth $\mathcal{L}_{\text{depth}}$. Even though the metrics are only slightly improved, adding this term helps to remove floating artifacts in the reconstructed scene. We include visualizations to support our statements in Supplementary Material.

5. Conclusion

In this work, we have presented novel *T-3DGS* method for 3D scene reconstruction using Gaussian Splatting by effectively removing foreground dynamic distractors from input videos. The key to the success are unsupervised classification network to identify transient distractors through novel consistency loss term and the mask propagation approach that improves the boundary and temporal consistency of the predicted transient masks. Our results show that our method achieves significant improvement over the state-of-the-art methods on densely captured videos populated with semi-transient distractors. We believe our method is a valuable contribution towards widespread usage of 3DGS for robust 3D scene reconstruction from real-world videos captured in uncontrolled settings.

T-3DGS: Removing Transient Objects for 3D Scene Reconstruction

Supplementary Material

A. Additional Implementation Details

For mask filtering and refinement in Sec. 3.3.1, we set $\lambda_{\text{cov}}^{\text{ref}} = 0.7$ for initial mask refinement and $\lambda_{\text{cov}}^{\text{val}} = 0.7$ for validation during object filtration. For temporal refinement in Sec. 3.3.2, we set the memory size parameter $N_m = 10$, which controls the number of frames considered during mask propagation. For the final mask dilation step, we perform $N_e = 5$ iterations of binary dilation. Also, the mask merging threshold λ_{merge} is set to 0.9, and the stability ratio threshold λ_{SR} to 0.08 in Sec. 3.3.3.

B. Evaluation on RobustNeRF Dataset

We provide evaluation on the *RobustNeRF* dataset [33]. As shown in Tab. 4 our method generally outperforms 3DGS [12], Robust 3DGS [43], WildGaussians [15], and shows similar performance comparing to SpotLessSplats [34]. We run our method directly on masks predicted by *TMP* module without mask propagator (*TMR*). In general, the dataset does not seem to be challenging enough to highlight the differences between different methods.

C. More Qualitative Comparisons

For qualitative comparison, we compare our method to SpotLessSplats [34] and Robust3DGS [43]. We provide corresponding renderings for the masks shown in the main paper in Sec. 4.2. Fig. 6 and 7 show reconstructions of several scenes from the *On-the-go* dataset on training and testing frames, respectively. Currently, most methods can produce fairly good reconstructions and avoid significant artifacts, so generally, most methods produce fairly similar results (at least in the absence of semi-transient objects and other adversarial cases). However, it is notable that compared to other residual-based methods, we avoid misclassifying high-frequency details and similar objects. This improvement can be attributed to our consistency loss term.

D. Additional Ablation Study

We provide visualizations that show the importance of each component in our proposed *T-3DGS* model on *On-the-go* dataset [31]. We show our ablation visualizations in Fig. 8 and 9.

E. Handling Semi-Transient Objects

Semi-transient objects have not been properly addressed in 3D scene reconstruction. Our method makes a large improvement over previous work and can handle fairly com-

plex scenarios. We provide some details about data capture and the methodology we employed with respect to semi-transient objects. We also discuss why both our consistency term as well as mask propagation are important for handling semi-transient objects. Additionally, we discuss some limitations of our proposed method.

Some scenes in our dataset include reduced and full versions - in the reduced scenes the camera operator goes from one end of the scene to the other, while for the full scenes they also retrace their path and return to their initial positions, while semi-transient objects kept moving. As seen in Fig. 10, our proposed *TMR* module is crucial to produce good results even for the reduced scenes, the more challenging scenario. For full scenes, the additional data significantly improves mask predictions for all models. We conclude that handling semi-transient objects is an important challenge for in-the-wild video processing. In order to provide the most challenging datasets and to rigorously compare different methods - one must consider not only the kinds of motion of dynamic objects, but also their movement with respect to the camera.

As mentioned above, some of the scenes include semi-transient objects occluding the static scene for prolonged periods of time while remaining mostly still. As this period of time increases, semi-transient objects can effectively become static. While this effect might seem irrelevant to the detection of dynamic objects, this is not the case. As shown in the Fig. 11, most methods mask static background as if it was masking the semi-transient object. Notably, our method avoids this problem, and this highlights the importance of using both the consistency term and mask propagation algorithm we introduced. While the consistency term alone may still misclassify semi-transient objects, we avoid false classifications of static objects as dynamic. Therefore, our consistency term is crucial in order for the mask propagation to avoid introducing additional errors. This is in stark contrast to the competing methods, which have a lot more false positives. Mask propagation would introduce additional errors and may not help improving the overall quality.

Our method reliably removes transient and semi-transient distractors and successfully reconstructs static artifact-free 3D scenes. However, we have noticed that predicted masks are inflated due to the low resolution of the extracted feature maps, our method can give inconsistent results for small objects, since DINOv2 features are computed on patches. These problems could be addressed by utilizing feature extractors with higher-resolution feature maps or guided upsampling. Additionally, the temporal refinement process is constrained by a memory window of N_m

	Android		Statue		Crab (1)		Crab (2)		Yoda		Mean	
	PSNR ↑	SSIM ↑										
NeRF On-the-go [31]	23.50	0.75	21.58	0.77	-	-	-	-	29.96	0.83	-	-
3DGS [12]	23.51	0.81	21.35	0.84	30.39	0.94	31.53	0.92	29.80	0.92	27.32	0.89
Robust 3DGS [43]	24.40	0.83	22.10	0.85	34.41	0.96	32.99	0.93	32.62	0.93	29.30	0.90
WildGaussians [15]	24.89	0.83	22.69	0.87	30.16	0.93	31.11	0.91	30.50	0.91	27.87	0.89
SpotLessSplats [34]	24.45	0.79	22.50	0.80	35.45	0.95	33.29	0.94	33.55	0.94	29.85	0.88
Ours	25.04	0.84	22.90	0.87	35.81	0.95	33.36	0.93	32.09	0.92	29.84	0.90

Table 4. Quantitative comparison on *RobustNeRF* dataset [33].

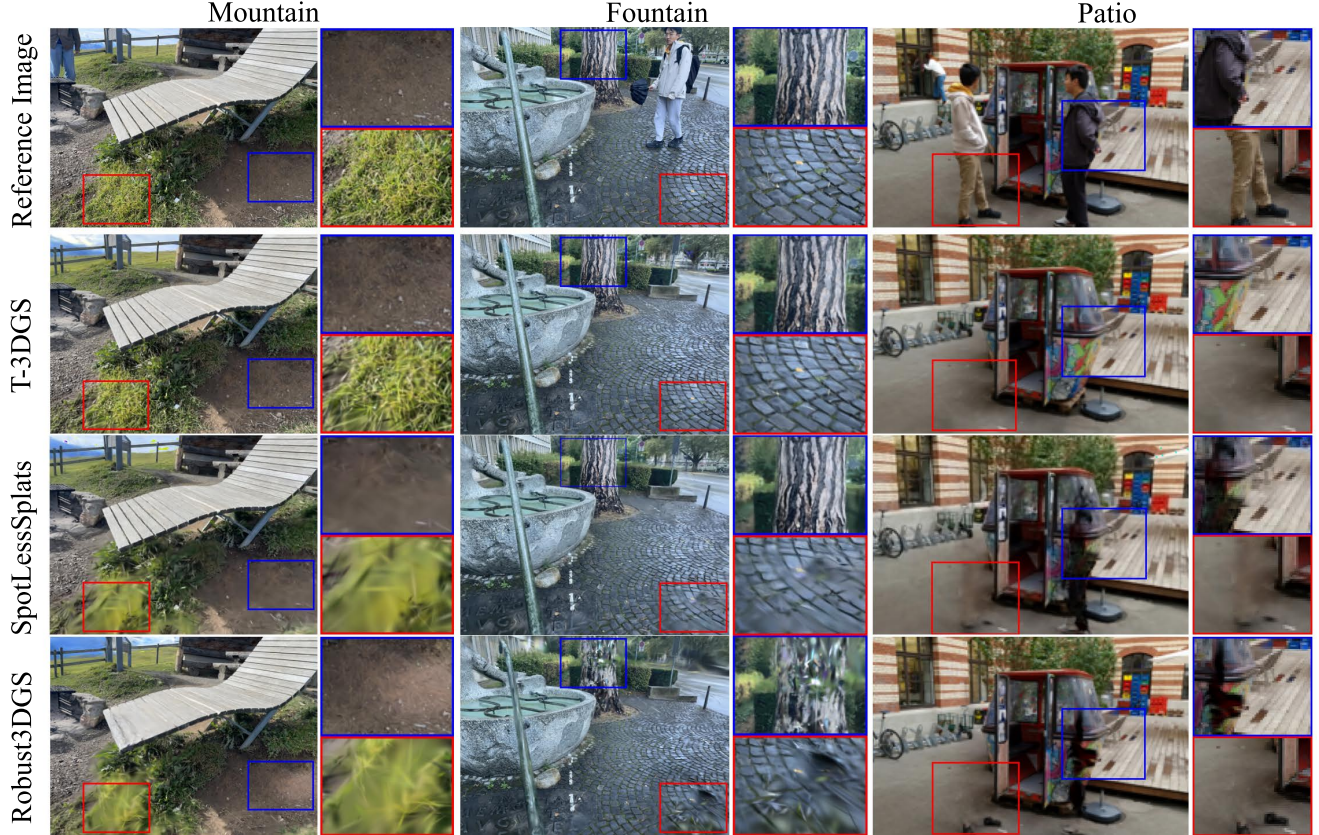


Figure 6. Qualitative results on *On-the-go* dataset on the training frames. Our method produces higher-quality renderings without artifacts.

frames, which means that if an object disappears for more than N_m frames and then reappears, it will be treated as a new instance with a different label. This can lead to inconsistent tracking and potentially affect the filtering process, especially for semi-transient objects that may temporarily leave the scene. Furthermore, our current filtering approach using global coverage scores may incorrectly filter out valid dynamic objects that undergo significant size changes, such as objects moving towards or away from the camera, or those experiencing perspective changes. We leave it as future work.

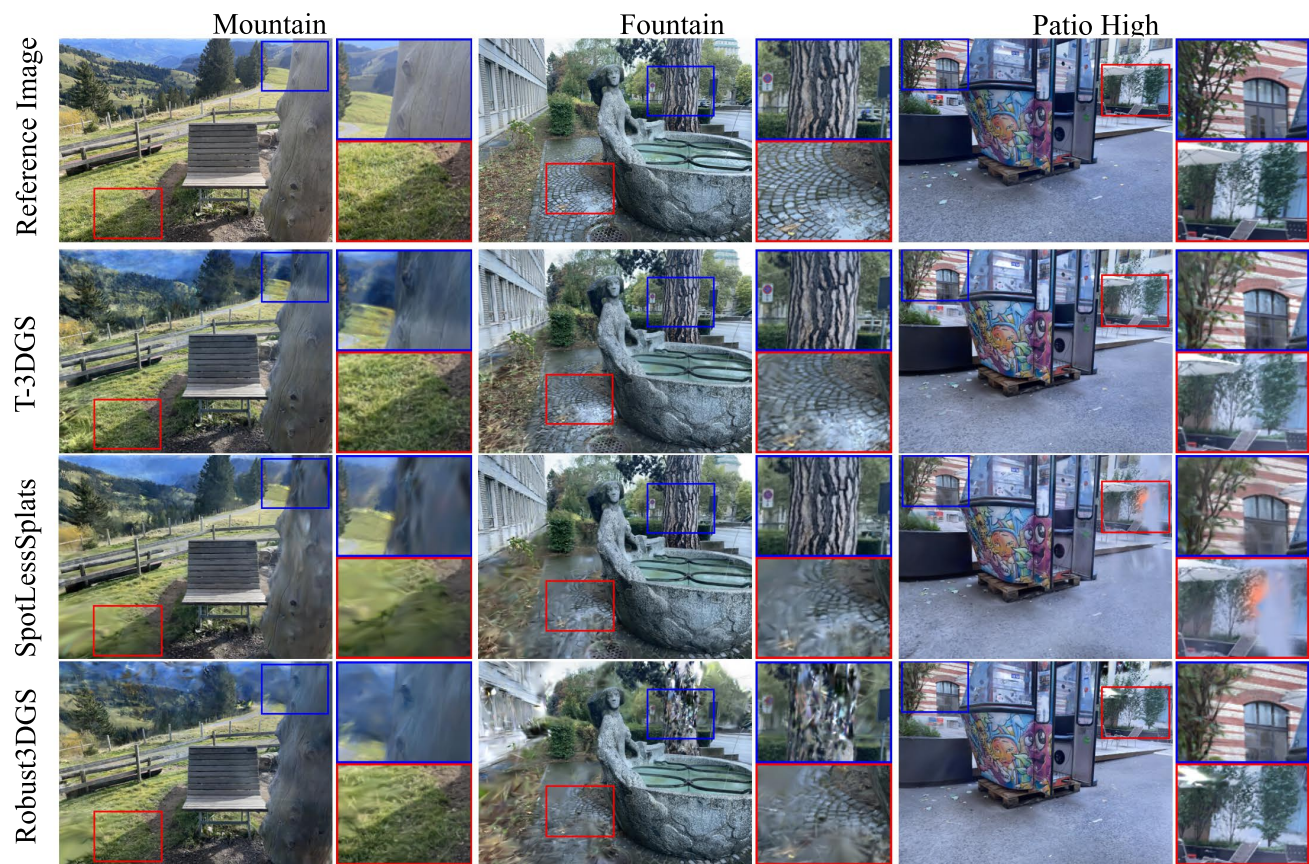


Figure 7. Qualitative results on *On-the-go* dataset on the testing frames. Our method produces higher-quality renderings without artifacts.

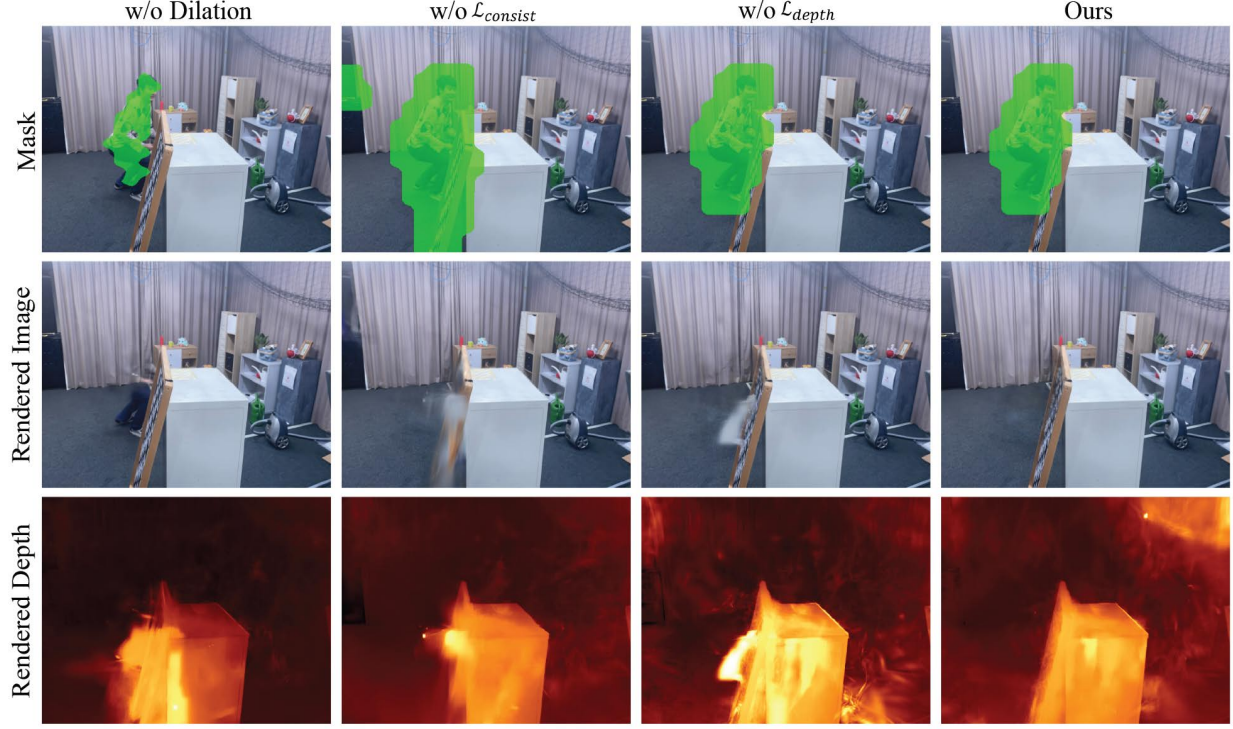


Figure 8. We ablate the importance of each component of our method on *On-the-go* dataset on Corner scene. We provide qualitative comparison for masks (row 1), rendered images (row 2), and rendered depths (row 3).

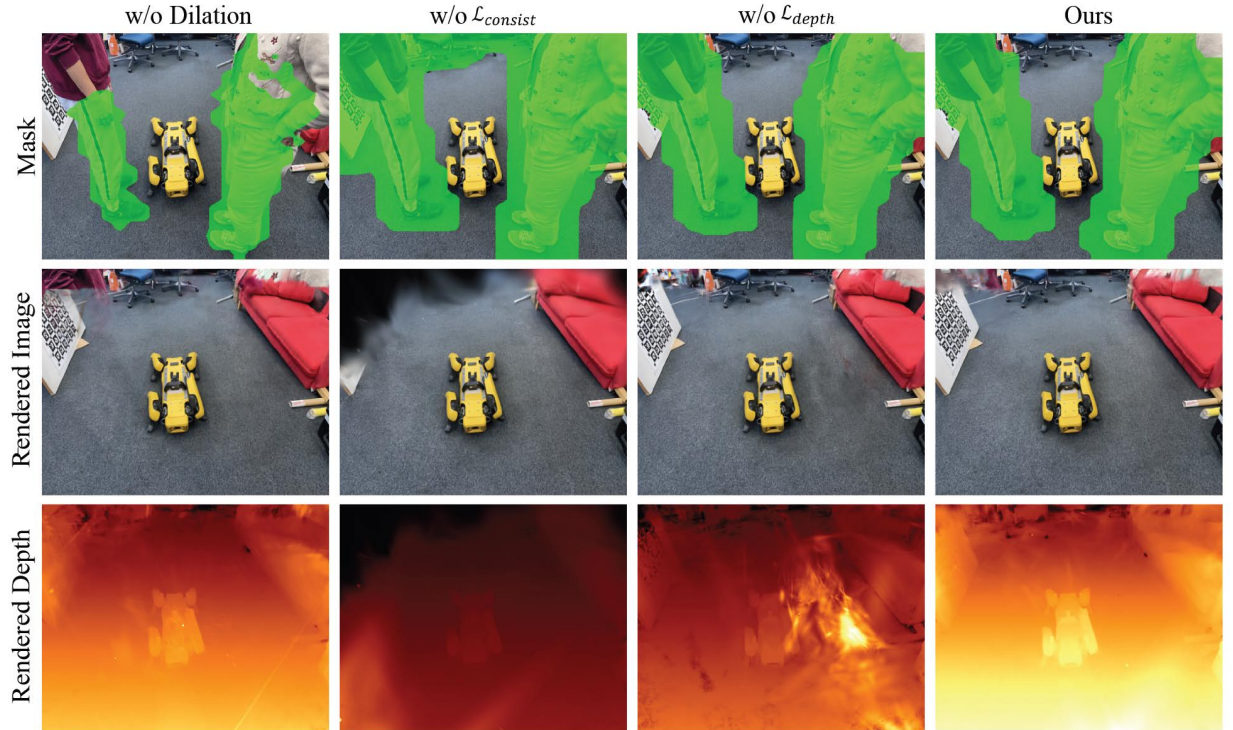


Figure 9. We ablate the importance of each component of our method on *On-the-go* dataset on Spot scene. We provide qualitative comparison for masks (row 1), rendered images (row 2), and rendered depths (row 3).

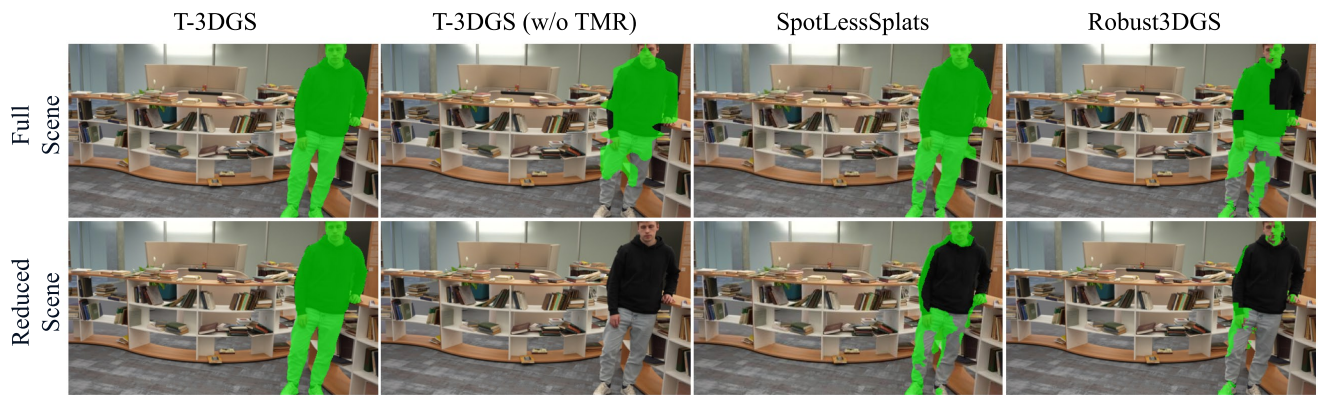


Figure 10. The comparison of predicted masks for full and reduced scenes.

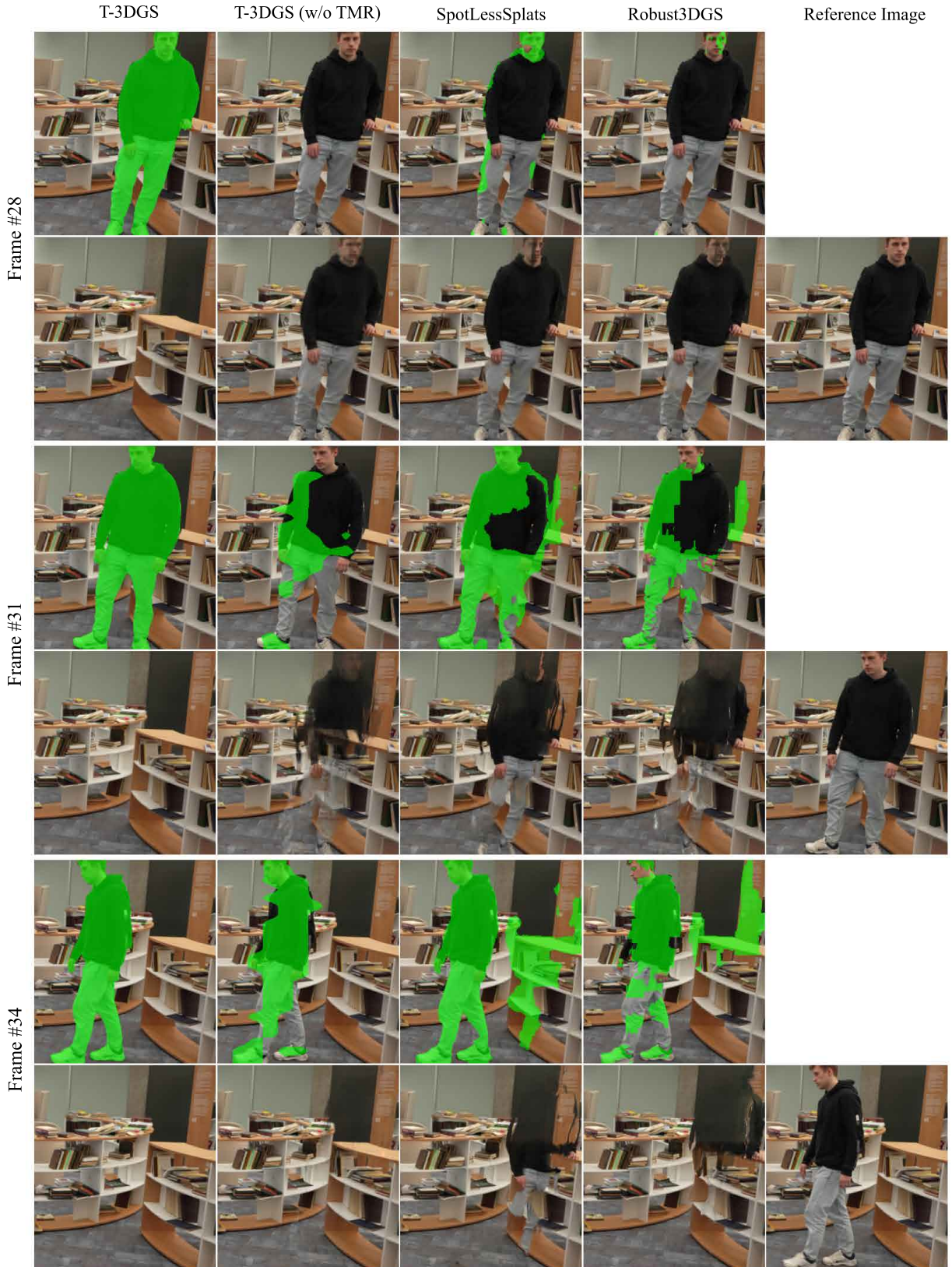


Figure 11. The comparison of predicted masks and scene reconstructions during movement of semi-transient objects for different frames.

References

- [1] Mathilde Caron, Hugo Touvron, Ishan Misra, Hervé Jégou, Julien Mairal, Piotr Bojanowski, and Armand Joulin. Emerging properties in self-supervised vision transformers. In *Proceedings of the IEEE/CVF international conference on computer vision*, pages 9650–9660, 2021. 3
- [2] Jiahao Chen, Yipeng Qin, Lingjie Liu, Jiangbo Lu, and Guanbin Li. Nerf-hugs: Improved neural radiance fields in non-static scenes using heuristics-guided segmentation. In *Proceedings of the IEEE/CVF Conference on Computer Vision and Pattern Recognition*, pages 19436–19446, 2024. 2
- [3] Zhiqin Chen, Thomas Funkhouser, Peter Hedman, and Andrea Tagliasacchi. Mobilenerf: Exploiting the polygon rasterization pipeline for efficient neural field rendering on mobile architectures. In *Proceedings of the IEEE/CVF Conference on Computer Vision and Pattern Recognition*, pages 16569–16578, 2023. 2
- [4] Ho Kei Cheng, Seoung Wug Oh, Brian Price, Alexander Schwing, and Joon-Young Lee. Tracking anything with decoupled video segmentation. In *Proceedings of the IEEE/CVF International Conference on Computer Vision*, pages 1316–1326, 2023. 3
- [5] Ho Kei Cheng, Seoung Wug Oh, Brian Price, Joon-Young Lee, and Alexander Schwing. Putting the object back into video object segmentation. In *Proceedings of the IEEE/CVF Conference on Computer Vision and Pattern Recognition*, pages 3151–3161, 2024. 3
- [6] Hiba Dahmani, Moussab Bennehar, Nathan Piasco, Luis Roldao, and Dzmitry Tsishkou. Swag: Splatting in the wild images with appearance-conditioned gaussians. *arXiv preprint arXiv:2403.10427*, 2024. 3, 4
- [7] Alexey Dosovitskiy, Lucas Beyer, Alexander Kolesnikov, Dirk Weissenborn, Xiaohua Zhai, Thomas Unterthiner, Mostafa Dehghani, Matthias Minderer, Georg Heigold, Sylvain Gelly, Jakob Uszkoreit, and Neil Houlsby. An image is worth 16x16 words: Transformers for image recognition at scale. *ICLR*, 2021. 3
- [8] Qiao Gu, Zhaoyang Lv, Duncan Frost, Simon Green, Julian Straub, and Chris Sweeney. Egolifter: Open-world 3d segmentation for egocentric perception. In *European Conference on Computer Vision*, pages 382–400. Springer, 2025. 4
- [9] Antoine Guédon and Vincent Lepetit. Sugar: Surface-aligned gaussian splatting for efficient 3d mesh reconstruction and high-quality mesh rendering. In *Proceedings of the IEEE/CVF Conference on Computer Vision and Pattern Recognition*, pages 5354–5363, 2024. 1
- [10] Jonathan Ho, Ajay Jain, and Pieter Abbeel. Denoising diffusion probabilistic models. *Advances in neural information processing systems*, 33:6840–6851, 2020. 3
- [11] Ajay Jain, Matthew Tancik, and Pieter Abbeel. Putting nerf on a diet: Semantically consistent few-shot view synthesis. In *Proceedings of the IEEE/CVF International Conference on Computer Vision*, pages 5885–5894, 2021. 2
- [12] Bernhard Kerbl, Georgios Kopanas, Thomas Leimkühler, and George Drettakis. 3d gaussian splatting for real-time radiance field rendering. *ACM Trans. Graph.*, 42(4):139–1, 2023. 1, 2, 3, 7, 9, 10
- [13] Justin Kerr, Chung Min Kim, Ken Goldberg, Angjoo Kanazawa, and Matthew Tancik. Lerf: Language embedded radiance fields. In *Proceedings of the IEEE/CVF International Conference on Computer Vision*, pages 19729–19739, 2023. 1
- [14] Alexander Kirillov, Eric Mintun, Nikhila Ravi, Hanzi Mao, Chloe Rolland, Laura Gustafson, Tete Xiao, Spencer Whitehead, Alexander C Berg, Wan-Yen Lo, et al. Segment anything. In *Proceedings of the IEEE/CVF International Conference on Computer Vision*, pages 4015–4026, 2023. 2, 3, 5
- [15] Jonas Kulhanek, Songyou Peng, Zuzana Kukelova, Marc Pollefeys, and Torsten Sattler. Wildgaussians: 3d gaussian splatting in the wild. *arXiv preprint arXiv:2407.08447*, 2024. 4, 5, 7, 9, 10
- [16] Zhaoshuo Li, Thomas Müller, Alex Evans, Russell H Taylor, Mathias Unberath, Ming-Yu Liu, and Chen-Hsuan Lin. Neuralangelo: High-fidelity neural surface reconstruction. In *Proceedings of the IEEE/CVF Conference on Computer Vision and Pattern Recognition*, pages 8456–8465, 2023. 1
- [17] Zhuang Liu, Hanzi Mao, Chao-Yuan Wu, Christoph Feichtenhofer, Trevor Darrell, and Saining Xie. A convnet for the 2020s. In *Proceedings of the IEEE/CVF conference on computer vision and pattern recognition*, pages 11976–11986, 2022. 3
- [18] Grace Luo, Lisa Dunlap, Dong Huk Park, Aleksander Holynski, and Trevor Darrell. Diffusion hyperfeatures: Searching through time and space for semantic correspondence. *Advances in Neural Information Processing Systems*, 36, 2024. 3
- [19] Ricardo Martin-Brualla, Noha Radwan, Mehdi SM Sajjadi, Jonathan T Barron, Alexey Dosovitskiy, and Daniel Duckworth. Nerf in the wild: Neural radiance fields for unconstrained photo collections. In *Proceedings of the IEEE/CVF conference on computer vision and pattern recognition*, pages 7210–7219, 2021. 2
- [20] Hidenobu Matsuki, Riku Murai, Paul HJ Kelly, and Andrew J Davison. Gaussian splatting slam. In *Proceedings of the IEEE/CVF Conference on Computer Vision and Pattern Recognition*, pages 18039–18048, 2024. 2
- [21] Ben Mildenhall, Pratul P Srinivasan, Matthew Tancik, Jonathan T Barron, Ravi Ramamoorthi, and Ren Ng. Nerf: Representing scenes as neural radiance fields for view synthesis. *Communications of the ACM*, 65(1):99–106, 2021. 1, 2
- [22] Thomas Müller, Alex Evans, Christoph Schied, and Alexander Keller. Instant neural graphics primitives with a multiresolution hash encoding. *ACM transactions on graphics (TOG)*, 41(4):1–15, 2022. 2
- [23] Maxime Oquab, Timothée Darcet, Théo Moutakanni, Huy Vo, Marc Szafraniec, Vasil Khalidov, Pierre Fernandez, Daniel Haziza, Francisco Massa, Alaaeldin El-Nouby, et al. Dinov2: Learning robust visual features without supervision. *arXiv preprint arXiv:2304.07193*, 2023. 2, 3, 4
- [24] Keunhong Park, Utkarsh Sinha, Jonathan T Barron, Sofien Bouaziz, Dan B Goldman, Steven M Seitz, and Ricardo

- Martin-Brualla. Nerfies: Deformable neural radiance fields. In *Proceedings of the IEEE/CVF International Conference on Computer Vision*, pages 5865–5874, 2021. 2
- [25] Ben Poole, Ajay Jain, Jonathan T Barron, and Ben Mildenhall. Dreamfusion: Text-to-3d using 2d diffusion. *arXiv preprint arXiv:2209.14988*, 2022. 1
- [26] Albert Pumarola, Enric Corona, Gerard Pons-Moll, and Francesc Moreno-Noguer. D-nerf: Neural radiance fields for dynamic scenes. In *Proceedings of the IEEE/CVF Conference on Computer Vision and Pattern Recognition*, pages 10318–10327, 2021. 2
- [27] Alec Radford, Jong Wook Kim, Chris Hallacy, Aditya Ramesh, Gabriel Goh, Sandhini Agarwal, Girish Sastry, Amanda Askell, Pamela Mishkin, Jack Clark, et al. Learning transferable visual models from natural language supervision. In *International conference on machine learning*, pages 8748–8763. PMLR, 2021. 3
- [28] Ravi Ramamoorthi and Pat Hanrahan. An efficient representation for irradiance environment maps. In *Proceedings of the 28th annual conference on Computer graphics and interactive techniques*, pages 497–500, 2001. 3
- [29] Nikhila Ravi, Valentin Gabeur, Yuan-Ting Hu, Ronghang Hu, Chaitanya Ryali, Tengyu Ma, Haitham Khedr, Roman Rädele, Chloe Rolland, Laura Gustafson, et al. Sam 2: Segment anything in images and videos. *arXiv preprint arXiv:2408.00714*, 2024. 3, 6
- [30] Daniel Rebain, Mark Matthews, Kwang Moo Yi, Dmitry Lagun, and Andrea Tagliasacchi. Lolnerf: Learn from one look. In *Proceedings of the IEEE/CVF Conference on Computer Vision and Pattern Recognition*, pages 1558–1567, 2022. 2
- [31] Weining Ren, Zihan Zhu, Boyang Sun, Jiaqi Chen, Marc Pollefeys, and Songyou Peng. Nerf on-the-go: Exploiting uncertainty for distractor-free nerfs in the wild. In *Proceedings of the IEEE/CVF Conference on Computer Vision and Pattern Recognition*, pages 8931–8940, 2024. 2, 7, 9, 10
- [32] Robin Rombach, Andreas Blattmann, Dominik Lorenz, Patrick Esser, and Björn Ommer. High-resolution image synthesis with latent diffusion models. In *Proceedings of the IEEE/CVF conference on computer vision and pattern recognition*, pages 10684–10695, 2022. 3
- [33] Sara Sabour, Suhani Vora, Daniel Duckworth, Ivan Krasin, David J Fleet, and Andrea Tagliasacchi. Robustnerf: Ignoring distractors with robust losses. In *Proceedings of the IEEE/CVF Conference on Computer Vision and Pattern Recognition*, pages 20626–20636, 2023. 2, 7, 9, 10
- [34] Sara Sabour, Lily Goli, George Kopanas, Mark Matthews, Dmitry Lagun, Leonidas Guibas, Alec Jacobson, David J Fleet, and Andrea Tagliasacchi. Spotlesssplats: Ignoring distractors in 3d gaussian splatting. *arXiv preprint arXiv:2406.20055*, 2024. 1, 2, 3, 4, 7, 8, 9, 10
- [35] Johannes L Schonberger and Jan-Michael Frahm. Structure-from-motion revisited. In *Proceedings of the IEEE conference on computer vision and pattern recognition*, pages 4104–4113, 2016. 2
- [36] Jin-Chuan Shi, Miao Wang, Hao-Bin Duan, and Shao-Hua Guan. Language embedded 3d gaussians for open-vocabulary scene understanding. In *Proceedings of the IEEE/CVF Conference on Computer Vision and Pattern Recognition*, pages 5333–5343, 2024. 1
- [37] Yawar Siddiqui, Lorenzo Porzi, Samuel Rota Buló, Norman Müller, Matthias Nießner, Angela Dai, and Peter Kortscheder. Panoptic lifting for 3d scene understanding with neural fields. In *Proceedings of the IEEE/CVF Conference on Computer Vision and Pattern Recognition*, pages 9043–9052, 2023. 1
- [38] Cheng Sun, Min Sun, and Hwann-Tzong Chen. Direct voxel grid optimization: Super-fast convergence for radiance fields reconstruction. In *Proceedings of the IEEE/CVF conference on computer vision and pattern recognition*, pages 5459–5469, 2022. 2
- [39] Jiaxiang Tang, Zhaoxi Chen, Xiaokang Chen, Tengfei Wang, Gang Zeng, and Ziwei Liu. Lgm: Large multi-view gaussian model for high-resolution 3d content creation. In *European Conference on Computer Vision*, pages 1–18. Springer, 2025. 1
- [40] Luming Tang, Menglin Jia, Qianqian Wang, Cheng Perng Phoo, and Bharath Hariharan. Emergent correspondence from image diffusion. *Advances in Neural Information Processing Systems*, 36:1363–1389, 2023. 3, 4
- [41] Hugo Touvron, Matthieu Cord, Matthijs Douze, Francisco Massa, Alexandre Sablayrolles, and Hervé Jégou. Training data-efficient image transformers & distillation through attention. In *International conference on machine learning*, pages 10347–10357. PMLR, 2021. 3
- [42] Edgar Tretschk, Ayush Tewari, Vladislav Golyanik, Michael Zollhöfer, Christoph Lassner, and Christian Theobalt. Non-rigid neural radiance fields: Reconstruction and novel view synthesis of a dynamic scene from monocular video. In *Proceedings of the IEEE/CVF International Conference on Computer Vision*, pages 12959–12970, 2021. 2
- [43] Paul UngermaNN, Armin Ettenhofer, Matthias Nießner, and Barbara Roessle. Robust 3d gaussian splatting for novel view synthesis in presence of distractors. *arXiv preprint arXiv:2408.11697*, 2024. 2, 3, 7, 8, 9, 10
- [44] Peng Wang, Lingjie Liu, Yuan Liu, Christian Theobalt, Taku Komura, and Wenping Wang. Neus: Learning neural implicit surfaces by volume rendering for multi-view reconstruction. *arXiv preprint arXiv:2106.10689*, 2021. 1
- [45] Zhou Wang, Alan C Bovik, Hamid R Sheikh, and Eero P Simoncelli. Image quality assessment: from error visibility to structural similarity. *IEEE transactions on image processing*, 13(4):600–612, 2004. 7
- [46] Frederik Warburg, Ethan Weber, Matthew Tancik, Aleksander Holynski, and Angjoo Kanazawa. Nerfbusters: Removing ghostly artifacts from casually captured nerfs. In *Proceedings of the IEEE/CVF International Conference on Computer Vision*, pages 18120–18130, 2023. 2
- [47] Guanjun Wu, Taoran Yi, Jiemin Fang, Lingxi Xie, Xiaopeng Zhang, Wei Wei, Wenyu Liu, Qi Tian, and Xinggang Wang. 4d gaussian splatting for real-time dynamic scene rendering. In *Proceedings of the IEEE/CVF Conference on Computer Vision and Pattern Recognition*, pages 20310–20320, 2024. 2
- [48] Jamie Wynn and Daniyar Turmukhambetov. Diffusionerf: Regularizing neural radiance fields with denoising diffu-

- sion models. In *Proceedings of the IEEE/CVF Conference on Computer Vision and Pattern Recognition*, pages 4180–4189, 2023. 1
- [49] Jiacong Xu, Yiqun Mei, and Vishal M Patel. Wild-gs: Real-time novel view synthesis from unconstrained photo collections. *arXiv preprint arXiv:2406.10373*, 2024. 3, 4
- [50] Chi Yan, Delin Qu, Dan Xu, Bin Zhao, Zhigang Wang, Dong Wang, and Xuelong Li. Gs-slam: Dense visual slam with 3d gaussian splatting. In *Proceedings of the IEEE/CVF Conference on Computer Vision and Pattern Recognition*, pages 19595–19604, 2024. 2
- [51] Lihe Yang, Bingyi Kang, Zilong Huang, Xiaogang Xu, Jiashi Feng, and Hengshuang Zhao. Depth anything: Unleashing the power of large-scale unlabeled data. In *Proceedings of the IEEE/CVF Conference on Computer Vision and Pattern Recognition*, pages 10371–10381, 2024. 3
- [52] Zeyu Yang, Hongye Yang, Zijie Pan, and Li Zhang. Real-time photorealistic dynamic scene representation and rendering with 4d gaussian splatting. *arXiv preprint arXiv:2310.10642*, 2023. 2
- [53] Dongbin Zhang, Chuming Wang, Weitao Wang, Peihao Li, Minghan Qin, and Haoqian Wang. Gaussian in the wild: 3d gaussian splatting for unconstrained image collections. *arXiv preprint arXiv:2403.15704*, 2024. 3
- [54] Junyi Zhang, Charles Herrmann, Junhwa Hur, Luisa Polania Cabrera, Varun Jampani, Deqing Sun, and Ming-Hsuan Yang. A tale of two features: Stable diffusion complements dino for zero-shot semantic correspondence. *Advances in Neural Information Processing Systems*, 36, 2024. 3
- [55] Zehao Zhu, Zhiwen Fan, Yifan Jiang, and Zhangyang Wang. Fsgs: Real-time few-shot view synthesis using gaussian splatting. In *European Conference on Computer Vision*, pages 145–163. Springer, 2025. 2